agronomy

MDPI

Article

A Monthly Water Balance Model for Vineyard Planning and Inter-Row Management

Maria Costanza Andrenelli [1,*], Sergio Pellegrini [1], Claudia Becagli [1], Alessandro Orlandini [1], Rita Perria [2], Paolo Storchi [2] and Nadia Vignozzi [1]

[1] CREA—Research Centre Agriculture and Environment, Via di Lanciola, 12/A, 50125 Firenze, Italy; sergio.pellegrini@crea.gov.it (S.P.); claudia.becagli@crea.gov.it (C.B.); alessandro.orlandini@crea.gov.it (A.O.); nadia.vignozzi@crea.gov.it (N.V.)
[2] CREA—Research Centre Viticulture and Enology, Viale S. Margherita, 80, 52100 Arezzo, Italy; rita.perria@crea.gov.it (R.P.); paolo.storchi@crea.gov.it (P.S.)
* Correspondence: mariacostanza.andrenelli@crea.gov.it

Abstract: Vineyard is one of the most complex and vulnerable agroecosystems, and ongoing climate change makes it necessary to identify effective management and adaptation practices. For this reason, a water balance model tailored for viticulture was developed to be implemented within a Decision Support System (DSS) aimed at supporting winemakers both in the vineyard's planning and management phase. Starting from a simple monthly water balance, based on the Thornthwaite–Mather method, the model returns the water stress risk class through the connection to a soil and climate database; the user can however customize the response by inserting information related to a specific vineyard (e.g., planting, soil, and management layout). The model was tested using data from a three-year field experiment carried out in a vineyard under permanent grass cover (PG) or continuous tillage (CT), allowing for the evaluation of its performance in terms of water balance estimation. The model provided results consistent with the measured soil moisture values, and the annual risk of water stress corresponds to what was measured in the field, differing at most by only one class. The model can guide the user in finding the best solutions for designing new vineyards or managing the inter-row by simulating the adoption of different strategies (trellis system, planting density, type of cover crop or soil tillage) or suggesting alternative solutions (needs of irrigation supply, more suitable cultivars, or rootstocks).

Keywords: Thornthwaite–Mather method; vine phenology; soil management; vine water stress; evapotranspiration

Academic Editors: José Casanova Gascón and Paula Cristina Santana Paredes

Received: 15 November 2024
Revised: 21 December 2024
Accepted: 14 January 2025
Published: 18 January 2025

Citation: Andrenelli, M.C.; Pellegrini, S.; Becagli, C.; Orlandini, A.; Perria, R.; Storchi, P.; Vignozzi, N. A Monthly Water Balance Model for Vineyard Planning and Inter-Row Management. *Agronomy* **2025**, *15*, 233. https://doi.org/10.3390/agronomy15010233

1. Introduction

The vineyard undoubtedly represents one of the most complex Mediterranean agroecosystems, often associated with several environmental problems, amplified either by climate change or by the intensification of production techniques [1]. The expected prolonged dry periods and increasingly frequent extreme meteorological events caused by climate change could have significant impacts on viticulture [2,3]. In addition, since vineyards are frequently affected by erosion phenomena [4], and European policies through various actions [5,6], more sustainable agricultural practices, such as the adoption of cover crops are becoming more frequent due to their beneficial effect on multiple ecosystem services [7,8]. However, the association of cover crops with the vine is sometimes questioned due to competition for water and nutrients.

As pointed out by Knowling et al. [9], despite the considerable development and availability of models for viticulture, their application in the context of vineyard management remains limited to the academic or research environment and the possibility of their use by the real agricultural world is remote.

For instance, in decision-making contexts, STICS [10] and VineLOGIC [11] models, due to their flexibility, could support the choice of planting layout and operational strategies such as canopy and water management.

However, like most open-source models available, both lack an easy-to-use graphical interface, and require specific skills, including the knowledge of both programming languages and processes implemented within the models, which neither the farmer nor the technical decision-maker possesses. In addition, they require quality and hard-to-find input data [12].

As a result, there are a few marketed (e.g., Terraclim [13], PreDiVine [14], Vite.net® [15]) and open-access models ready for wine growers or agronomist consultants to be employed within the vineyard decision-making process.

Regarding the design of the new vineyard, there is currently a complete lack of ready-to-use decision support models.

Although the vine is defined as a drought-tolerant species [16], large quantities of water are, however, necessary during the dry months to allow the plant to complete its growth cycle [17,18]. Young plants, in particular, are more sensitive to water shortage due to the fact their root system is not fully developed [19,20]; it is, therefore, crucial to evaluate the possible risk of water stress during the training stage right from the vineyard design phase. Gaining a better knowledge of soil hydrological behavior and, therefore, evaluating whether the crop water requirements along the different growth stages and for different soil management can be satisfied becomes crucial, especially in view of the ongoing climate change. Since the susceptibility of grapevine to water stress varies between the different phenological stages [21,22], the soil moisture data alone, expressed as potential (SWP), is not able to provide useful indications about the stress level of the plant [23,24]. Therefore, to define the vine tolerance thresholds for each phenological phase, the pre-dawn leaf water potential was used since it is assumed to be in equilibrium with the soil water potential (SWP) [21]. The monthly step water balance model is successfully employed to provide a basis for decision-support systems in the context of water management [25]. As outlined by Hong et al. [26], these monthly based water balance models have been proposed during the last few decades with the aim of improving their physical basis without excessively increasing their complexity and the need for a huge quantity of input data. Among these models, Mammoliti et al. [27] identify the Thornthwaite–Mather method [28] as one of the most used, especially for hydrogeological purposes, because it is simple but able to provide reliable outputs. For this reason, Mammoliti et al. [27] implemented a WebApp for the automatic calculation of Thornthwaite—Mather water balance, able to carry out the computation on large datasets. Given its wide use, many improvements to the Thornthwaite–Mather method have been carried out over time by several authors to adequately respond to their specific needs. Hence, new information about soils, crop, management, or climate have been included, and properly modeled, by different authors [29–32]. This work illustrates a modified Thornthwaite–Mather water balance model, that is able to assess the risk of water stress in the various phenological phases before and during the productive age. Starting from the spreadsheet elaborated by Armiraglio et al. [33], several procedural changes, functional to the application of the soil water balance within a DSS aimed at supporting farmers in the vineyard's planning and management, have been made. The model provides as output the water stress risk class, so allowing (a) to forecast the need for irrigation supply in young vineyards, (b) support

the farmer in the choice of trellis system, planting density, cultivar, and rootstock, and (c) suggest the inter-row management system for achieving most suitable production objectives. The model was tested using data from a three-year field experiment (2020–2022), which was carried out in a vineyard under permanent grass cover (PG) or continuous tillage (CT), allowing for the evaluation of its performance in terms of water balance estimation and the effect of water stress on some production parameters. Finally, the application of the model in the planning of new vineyards under a future climatic scenario (2021–2050) is illustrated.

2. Materials and Methods

2.1. Model Description

In its original version, Thornthwaite's water balance [28] uses an extremely simple calculation procedure capable of allocating among the various components of the hydrological system, on a monthly basis, the volume of water stored in the various components of the landscape. The model's inputs are the mean monthly air temperature and precipitation, as well as soil hydrological properties (water content at field capacity—FC; and wilting point—WP), and the latitude of the site to account for the day length. Changes in soil moisture storage can be generalized as a result of the balance between the amount of water inputs and outputs. Inputs include precipitation and capillary rise; the outputs are direct runoff, deep percolation, and evapotranspiration. The capillary rise is assumed to be negligible. Only the changes made to the individual components of the water balance are illustrated hereafter, whereas the computational steps that have not undergone changes or updates are described in detail in Appendix A.

2.1.1. Water Surplus: Direct Runoff and Deep Percolation

In the procedure of Armiraglio et al. [33], the surplus occurs solely when the soil has already reached the field capacity and represents the overall water loss for direct runoff and deep percolation, according to Thornthwaite and Mather' method [34]. Direct runoff represents the amount of rainfall that does not participate in the recharge of soil water storage; that is, it is the quantity of precipitation that does not infiltrate into the soil [35]. In McCabe et al. [36], conversely, the direct runoff is a fixed value equal to 5% of the rainfall regardless of soil properties and previous soil water content. Following the procedure of Ferguson [37], the direct runoff was determined by the Soil Conservation Service Curve Number (SCS-CN) method [38]. In this way, based on the hydrological characteristics of the soil and the management system of the vineyard, the amount of rainfall lost as direct runoff was quantified monthly. To apply the SCS method, curve number (CN) values for different soils and management systems were determined. For each soil type, the hydrological soil group (HSG) was identified and, successively, CN values for PG and CT management were chosen from Roux et al. [39]. Regarding green manure (GM) management, CN value was determined, month by month, combining CN values of both PG and CT, that is, considering the different degrees of soil cover during the periods in which vegetation is present or not.

In each month, the net rainfall (P_{net}) is then given by:

$$P_{net} = P - Direct\ Runoff \quad (1)$$

Deep percolation represents the unknown variable in the water balance approach where the known components are rainfall, evapotranspiration, direct runoff and soil moisture change [40]. Therefore, it has been calculated month by month as residual of the soil water balance, that is subtracting the direct runoff from the overall water surplus.

2.1.2. Potential Evapotranspiration (PE)

The monthly potential evapotranspiration (PE) is calculated by Equation (A1) in Appendix A; later, PE is multiplied by two coefficients, ***k*** and ***s***, respectively, to account for the real length of the month and the theoretical sunshine hours, as well as for the actual sunbathing, depending on the latitude, slope, and aspect of the site [33]. ***s*** is determined following the procedure illustrated in the VSIM User Guide [41]. Furthermore, since in the VSIM model the variations in radiation are calculated starting from the daily declination values, to implement the same procedure on a monthly time step, each month is associated with a single declination value, i.e., the one relating to the fifteenth day.

Finally, the revised monthly potential evapotranspiration value (*PEc*), expressed in mm, is calculated by the following equation:

$$PEc = PE \times k \times s \quad (2)$$

2.1.3. Actual Evapotranspiration

The water demand of the vineyard is modeled according to the vigor of the plant, its phenological stage, and the different inter-row management system (i.e., PG, GM, or CT). For this purpose, two different crop coefficients are used, *kc* (vine) and *kcc* (cover crop): both depend on the vineyard characteristics, specifically LAI and cover crop coverage, but also on the monthly soil water availability.

The peak LAI value is simply determined from the Exposed Leaf Area (*ELA*, $m^2\ ha^{-1}$) [42], computable through a geometrical approach by applying the following formula:

$$ELA = \frac{c}{100} \times (2 \times H_l + D) \times \left(\frac{10,000}{E}\right) \quad (3)$$

where H_l is the leaf wall height (m), D is its thickness (m), E is the distance between the rows (m), and ***c*** is the canopy density (%).

Then, peak *LAI* ($m^2\ m^{-2}$) is estimated by the following equation:

$$LAI = \frac{(ELA)}{10,000} \quad (4)$$

The model foresees the vertical trellis (cordon system) as the default setting and uses specific geometric characteristics (Table 1). In the case of young plants, *c* is set equal to 50%. A similar geometrical approach is employed to compute peak *LAI* values for other trellis systems (see Appendix A).

Table 1. Values of the main geometric parameters and coefficients used to run the model in the case of young or mature vineyards. E = distance between rows; D = Trellis thickness; c = percentage canopy density; H_l = leaf wall height; *LAI* = Leaf Area Index; kc_M = maximum value of vine crop coefficient; R = cover crop width; P = percentage of vegetation cover; and kcc_M = maximum value of cover crop coefficient.

Vineyard	***E*** **(m)**	***D*** **(m)**	$\boldsymbol{H_l}$ **(m)**	***c*** **(%)**	***LAI*** **($m^2\ m^{-2}$)**	$\boldsymbol{kc_M}$	**R (m)**	**P (%)**	$\boldsymbol{kcc_M}$
Young	2.00	0.40	1.00	50	0.60	0.324	-	0	0.000
Mature	2.00	0.40	1.00	100	1.20	0.513	1.50	75	0.562

Vine Crop Coefficient (Kc)

Following the procedure adopted in the VSIM User Guide [41], the maximum value of the vine *kc* (kc_M) is computed by applying the Beer's Law, setting the light extinction coefficient to 0.6 according to Pierce et al. [41]:

$$kc_M = 1 - Exp(-0.6 \times peak\ LAI) \quad (5)$$

The reconstruction of the crop coefficient curve, based on the vine phenological phases from April to November, was carried out following the FAO method [43].

Vineyard Management

The crop coefficient in the case of CT was set constant and was equal to zero; conversely, the maximum value of the cover crop coefficient *kcc* was used for both GM and PG, and estimated in terms of both density and extension of vegetation cover. So, the percentage of soil surface covered by the cover crop and the proportion between the inter-row width occupied by vegetation and the whole inter-row width were considered. The maximum value of *kcc* (kcc_M) is calculated by the following equation:

$$kcc_M = \left(\frac{p}{100}\right) \times \left(\frac{R}{E}\right) \quad (6)$$

where p is the percentage of the soil surface covered by vegetation, R is the cover crop width on the inter-row (m), and E is the inter-row width (m).

If the user does not provide specific information, the default conditions are set to p = 75%, R = 1.5 m and E = 2 m.

The attribution of *kccj* values in the different months depends on the type of cover crop used: for PG, *kccj* is set constant and equal to the maximum value, unless the water stress condition occurs. In the case of GM, the *kccj* values depend on the phenology of the cover crop used: for this reason, the sequence of *kccj* values was reconstructed, assuming that the sowing and burial operations are carried out in October and June, respectively.

In addition, according to the procedure described in the VSIM Guide [41], *kccj* was adjusted in relation to soil moisture condition: it is reduced linearly with soil moisture of the antecedent month, reaching the maximum value when the soil is at the field capacity (FC) and being zero when soil moisture reaches 60% of FC (see Equation (A11) in Appendix A).

By multiplying the monthly value of the potential evapotranspiration (PEc_j) corrected by the addition of both the crop coefficients (vine and cover crop, if any), the actual Evapotranspiration (Etc_j) is computed for every *j*-month as follows:

$$Etc_j = PEc_j \times \left(kc_j + kcc_j\right) \quad (7)$$

2.1.4. Soil Water Storage Computation and Dynamics

Maximum Soil Water Storage (AWC)

The soil water storage (ST), expressed in mm, quantifies the water amount available to plants (i.e., vine and cover crop, when present) within soil rooting depth (Rd), set at the most equal to 0.75 m, regardless of cultivar and rootstock. If a soil is shallower than 0.75 m, the model considers the actual soil depth, otherwise it sets the Rd = 0.75 m. ST depends on many factors: soil characteristics (physical and hydrological), vineyard management (tillage and cover crop), and climatic regime at a given time. In the model, the maximum value of ST coincides with the Available Water Capacity (AWC), obtained by adding the differences between values of water content at Field Capacity (FC_i) and Wilting Point (WP_i)

of all the soil horizons identified between the surface and Rd. In the case of young plants, Rd is set equal to 0.35 m.

When water retention curve data are not available, FC_i and WP_i (cm^3 cm^{-3}) are determined through the equations elaborated by Saxton et al. [30].

Provided that ST is given in mm, FC_i and WP_i values must be converted into mm through the following equations:

$$FC_{i(mm)} = \frac{FC_i}{100} \times \left(1 - \frac{SK_i}{100}\right) h_i;\ WP_{i(mm)} = \frac{WP_i}{100} \times \left(1 - \frac{SK_i}{100}\right) h_i; \quad (8)$$

where SK_i is the skeleton content (%vol), and h_i (mm) the thickness of the i-th layer.

Soil Water Dynamics

The approach simulates the monthly soil water storage dynamics (ST) according to the hydrological bucket model implemented in Armiraglio et al. [23]; the only exception is the use of net rainfall (P_{net}) instead of total rainfall (P), and the separation of the water surplus into runoff and deep percolation. Briefly, when in the month j, the actual evapotranspiration (Etc_j) is larger than the P_{netj} soil water storage (ST_j); it undergoes a depletion, and otherwise increases up to the maximum water content, i.e., AWC. In any case, the extent of water storage also depends on the soil moisture status of the previous month. Beyond the AWC value, the water excess generates water surplus, that in turn will be divided into runoff and deep percolation depending on the hydrological properties of the soil (SCS-CN Method) [38]. In Appendix A, the Equations (Equations (A1)–(A18)) employed for modeling soil water dynamics are listed and explained.

2.1.5. Vine Water Stress Assessment

The model considers the specific water stress tolerance of the vine in the different phenological phases of both young (1–3 years after planting) and mature plants. To relate the water status of the vine to the soil moisture content, the pre-dawn leaf water potential value was used since it is assumed, as suggested by Deloire et al. [24], that this is in equilibrium with the soil water potential (SWP). This means that it is possible to use soil water content value (SM), converted into potential and expressed as MPa (SWP), to define the vine water status.

Namely, monthly soil water contents up to the rooting depth Rd (mm) were computed by adding the WP value (mm) to monthly ST values (mm), i.e., the model output. Hence, SM spans from a maximum level equal to FC and a hypothetical minimum value coincident with WP.

To convert SM values (mm) into SWP (MPa), the equation of Saxton et al. [44] was employed (see Equation (A15) Appendix A).

The tolerance of vines, both young and mature, to water stress in the different months of the vegetative cycle and in the corresponding phenological phases has been related to specific ranges of SWP according to Ojeda [24] and Deloire et al. [21] (Table 2). For example, young plants are generally not tolerant to water stress, and the SWP should always be lower than 0.2 MPa; only in the maturation phase are the vines less sensitive to water stress.

Table 2. Scheme of vine water stress tolerance in each phenological phase for both young (a) and mature (b) vines.

Month	Apr	May	Jun 1 **	Jun 2 **	Jul	Aug	Sept	Oct	Nov
a									
Phenological phase	Bud break	Growth of vine shoot				Cane maturation			Falling of leaves and root growth
Tolerance	None	None				Moderate			None
SWP *	<0.2	<0.2				0.2–0.4			<0.2
b									
Phenological phase	Bud break and growth of vine shoot			Fruit set Veraison		Veraison Maturation			Falling of leaves and root growth
Tolerance	None			Moderate		High			Moderate
SWP *	<0.2			0.2–0.4		0.4–0.6			0.2–0.4

* SWP is expressed as absolute value (MPa), ** Jun 1 = first 15 days; Jun 2 = last 15 days.

Such a phenologically based soil water balance provides an expert judgment of the vine water stress level on a monthly basis, resulting from the intersection between SWP value with the vine water stress tolerance. A synthesis of the intersections for both the young and mature vineyards is shown in Table 3.

Table 3. Scheme of logically based intersection between soil water stress and vine water stress tolerance. The classes of vine stress risk are listed and defined as follows: VH = Very High, H = High, M = Moderate, and N = Negligible.

SWP (MPa)	Soil Water Stress	Vine Water Stress Tolerance		
		High	Moderate	None
>0.6	High	VH	VH	VH
0.6–0.4	Medium–High	M	H	VH
0.4–0.2	LightMedium	N	M	H
<0.2	Absent	N	N	N

Finally, the annual stress risk is given by an expert judgment that considers all the possible combinations of the nine monthly (April-November) vine stress risk classes. For that purpose, the scores 3, 2, 1, and 0 were assigned to the VH (Very High), H (High), M (Moderate), and N (Negligible) vine stress risk classes, respectively. By doing this, it is possible to add the scores of the nine combinations and obtain a numerical value that can theoretically span between 0, when all nine months are associated with the class (N), and 27 (3*9) in the case in which the very high stress (VH) risk is everywhere present. Four annual water stress risk classes were identified, as illustrated in Table 4, assuming that a score equal to 9 already represents a highly critical condition for the vine.

Table 4. Scores identifying the annual water stress risk classes.

Score	Class of Annual Water Stress Risk
>9	Very High
6–9	High
2–5	Moderate
<2	Negligible

2.2. Model Application at Vineyard and Farm Scale

The model was applied at vineyard scale with the aim to validate it. Later, once its robustness was verified, it was applied at the farm scale to demonstrate its possible use when planning new vineyards.

Both these activities were carried out in the Barone Ricasoli farm (about 250 ha), located in the Chianti Classico wine district (Tuscany, central Italy, municipality of Gaiole in Chianti, province of Siena, 43°23′21″ N, 11°26′24″ E), characterized by a high soil variability. The pedological map of the farm identifies the presence of 19 typological soil units (TSU) [45].

2.2.1. Model Application at Vineyard Scale: Set Up of the Experimental Site

A vineyard located at 445 m elevation on a moderate slope (18%), with a South–East aspect and up-and-down row orientation was selected to set up an experiment functional to test the model performance for different inter-row managements. Only one type of soil is present, called AGR1 (this TSU occupies the largest area, nearly 70 ha within the farm), and is classified as Skeleti Haplic Calcisols according to WRB (World Reference Base) system [46]. To this end, since 2015, the vineyard has been divided into two sub-areas, each five rows wide, under different soil management: continuous tillage (CT) and permanent grass cover in alternating rows (PG).

In the years 2020, 2021, and 2022, soil moisture and temperature were continuously monitored by 5TM sensors connected to an EM50 datalogger (Decagon), which was placed in the central row of each area at 0.35 and 0.55 m depths. Near each sensor control unit, a soil profile was dug and described according to WRB guidelines [46], and both disturbed and undisturbed soil samples were collected. Soil particle size distribution, was determined by using the Micromeritics Sedigraph 3100 apparatus [47], while the soil water retention curve was obtained by using a combination of the evaporation method (HYPROP, METER Group AG, München, Germany) and the chilled-mirror dew point equipment (Model WP4C, Decagon Devices, Inc., Pullman, WA, USA). Field moisture values were then converted into water potentials by Equation (A15) of Appendix A, entering coefficients A and B resulting from laboratory analyses.

In the same row and for both treatments (PG and CT), the survey of the grass coverage was carried out in triplicate by a 50 × 50 cm metallic frame and quantified according to Sanesi [48]. In addition, on five vines located in a symmetrical position with respect to the sensors, the measurement of trellis thickness (D) and leaf wall height (H_l) was carried out to calculate LAI.

During the trial period, some production components were measured; in each row, five consecutive plants were sampled to determine the production (kg/plant), the number (n) of bunches per plant, and the bunch and berry weight. In the winter period, the weight of the pruning wood was determined, and the Ravaz index was calculated [49]. A nearby weather station also provided daily climate data of the experimental area.

A comparison of the model performance is provided, either entering lab hydrological properties or estimates by pedotransfer functions (PTFs).

2.2.2. Application of the Model at Farm Scale: Simulations for Planning New Vineyards Under Future Climatic Scenario

With the aim of applying the model to the whole Barone Ricasoli farm, it was first necessary to collect the information regarding the geographical characteristics of each vineyard of the farm. Starting from a DTM with a 10 × 10 m resolution and the vector map of the farm's vineyards, statistics on altitude, slope, and aspects were obtained in the GIS environment for each vineyard. Then, satellite images were employed to assess the main row orientation and length of each vineyard. An example of the application of the model for the re-planting phase, supposing, for simplicity, to maintain the previous trellis system and plot geometry in all the vineyards is hereafter illustrated. Since a vineyard generally remains in production for at least thirty years, the climate scenario for 2021–2050 was chosen, and the global climate model RCP8.5 was used [50].

It should be emphasized that RCP8.5 represents a business-as-usual scenario, resulting from the failure to apply mitigation measures; therefore, considering the thirty-year period of 2021–2050 as the application time window, RCP8.5 can be considered a plausible choice [51]. Further information about the cultivar and planting system was kindly pro-

vided by the farm owners. In addition, a soil unit vector map containing data related to the soil physical properties needed by the model was employed [45].

Then, the hydrological constants (FC, WP, and AWC) of each soil unit were estimated by PTFs [44] and used to calculate the soil water storage up to the rooting depth of the young plants (0.35 m), following the procedure described in Section 2.1.4.

2.2.3. Statistics

The comparisons between the soil moisture measured in the field and the estimated values starting from the lab or PTFs hydrological constants were carried out by evaluating the percent differences between the three-year average value (2020, 2021, 2022) of the simulated water content for both treatments (PG and CT) compared to the soil field moisture value in each month.

After having checked this using the test of Shapiro–Wilk and Levene, as well as the assumptions of normality and homoscedasticity, respectively, data of production components were statistically analyzed by one-way ANOVA, using SPSS [52]. Differences were assumed to be statistically significant for $p < 0.05$.

3. Results and Discussion

3.1. Model Application at Vineyard Scale

3.1.1. Site and Soil Characteristics

During the three-year trial period, the climate recorded an increase in temperature with respect to the 30-year, 1991–2020 period, which registered an annual rainfall of 834 mm and an average temperature of 14 °C. In particular, the Aridity Index, according to Bagnouls–Gaussen [53], changed from humid to dry and very dry. The annual rainfall, which was around 1075 and 928 mm in 2020 and 2021, decreased to 721 mm in 2022; in the same year, the average annual temperature increased from 15 to 15.9 °C. Table 5 illustrates the main characteristics of each treatment.

Table 5. Average values of the main characteristics for both the continuous tillage (CT) and permanent grass cover (PG) treatment. E = distance between rows, D = Trellis thickness, H_l = leaf wall height, LAI = Leaf Area Index, kc_M = maximum value of vine crop coefficient, kcc_M = maximum value of cover crop coefficient, R = cover crop width, P = percentage of vegetation cover.

Treatment	E	D	H_l	LAI	kc_M	R	P	kcc_M
	(m)	(m)	(m)	(m^2 m^{-2})		(m)	(%)	
PG	2.0	0.33	0.94	1.11	0.49	1.5	45	0.34
CT	2.0	0.40	0.90	1.10	0.48	-	0.0	-

The main physical and hydrological soil properties entering the model, and the extreme values of soil moisture measured over the three years in the different treatments, are displayed in Table 6.

Table 6. Mean values of the main soil physical properties, along with the extreme field moisture values measured in the three years in both the treatments. For A, B, FC, and WP, both the values measured in lab, and those estimated by PTF (italic values) are reported. (HSG: hydrological soil group [38]; H: soil depth; SK: skeleton content; A and B: coefficients moisture tension [44]; FC: field capacity; WP: wilting point).

Treatment	HSG	H (m)	SK (%v)	Sand (%)	Clay (%)	Textural Class USDA	A	B	FC (mm)	WP (mm)	Max Field Moisture (mm)	Min Field Moisture (mm)
CT	C	0.75	30.7	31.5	21.4	L	*6.6×10^{-4}* 1.6×10^{-4}	*−4.98* −7.42	*148.9* 185.7	*79.6* 74.5	197.7	79.5
PG	D	0.75	22.6	22.5	27.6	CL	*7.0×10^{-4}* 8.6×10^{-5}	*−5.42* −7.85	*185.9* 202.7	*93.9* 77.9	210.5	130.0

Provided that the model ideally simulates monthly soil moisture content in the range between FC and WP, it is interesting to observe that laboratory analyses provide FC values comparable to the maximum moisture content measured in the field along the three-year period in both the treatments; vice versa, the FC values obtained by PTF are always lower (Table 6). In CT, all the WP values coincide with the minimum moisture content measured in the field. In PG, lab- and PTF-derived WP data differ from minimum field moisture by 28% to 40% (Table 6). It should be borne in mind that field soil moisture conditions can be out of the range and imposed by the model; therefore, theoretically, moisture above the FC can also be temporarily measured, and field conditions below the theoretical WP can exist. However, the monthly time scale adopted makes these situations in the field less likely and frequent (Figure 1a,b). In PG, although vegetation may be responsible for greater evapotranspiration, soil surface temperature remains lower, and moisture remains higher due to the protection that the vegetation cover exerts against solar radiation [54]. As a result, actual soil moisture values in PG may be higher in summer than those simulated by the model.

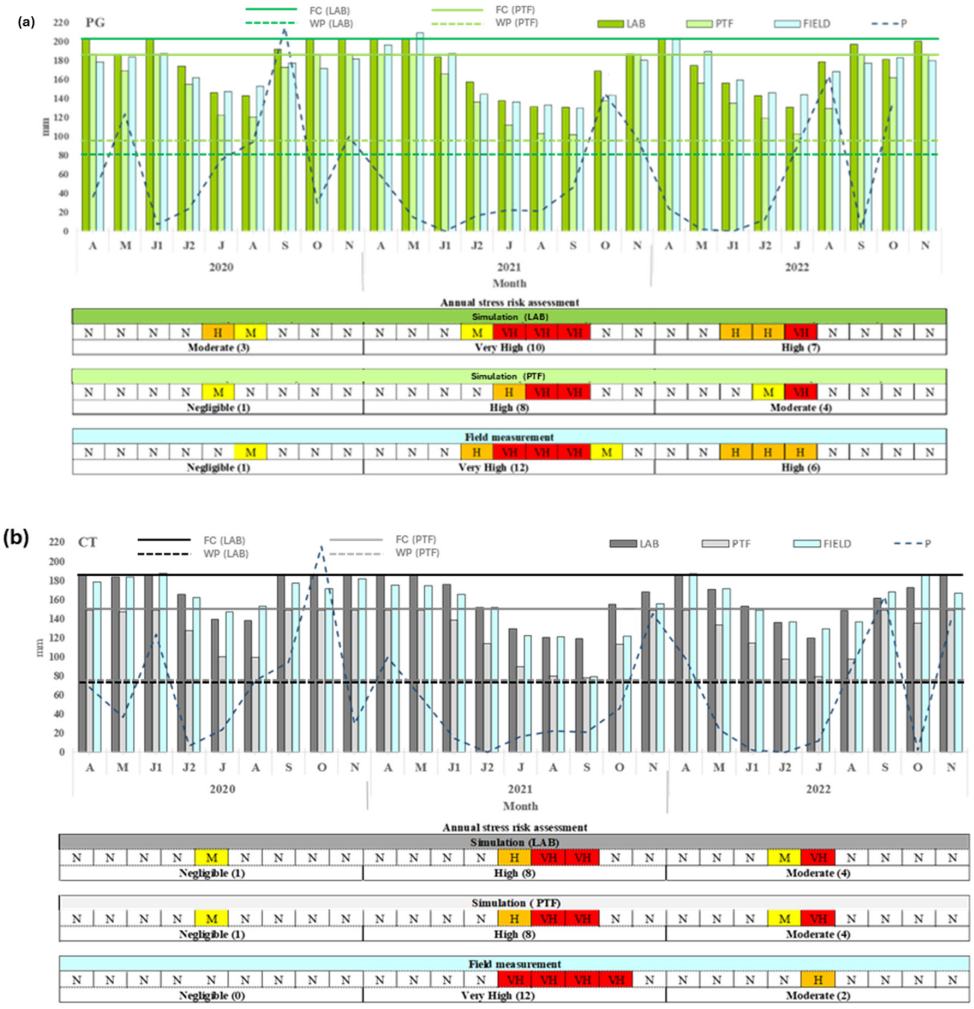

Figure 1. Model results for PG (permanent grass cover) (**a**) and CT (continuous tillage). (**b**) Management systems in the years 2020, 2021, and 2022. (P = precipitation; FIELD = soil moisture measured in the field; PTF = soil moisture estimated by the model entering the hydrological constants derived from PTFs; LAB = soil moisture estimated by the model entering the hydrological constants obtained by laboratory analyses; FC (LAB) and WP (LAB) = hydrological constants measured in the laboratory. FC (PTF) and WP (PTF) = hydrological constants estimated by PTFs.

3.1.2. Model Performance for the Experimental Site: Validation Results

The performance of the model with respect to the field soil moisture status is shown in Figure 1a,b, in which both the data obtained by model simulations and those measured in the PG and CT treatments in the three years (2020, 2021, and 2022) are displayed. The histograms show soil moisture monthly values (mm) measured in the field and those estimated by the model entering the hydrological constants derived from PTFs or laboratory analyses. The tables below each histogram show that the model results are related to the monthly and annual water stress risk assessment.

In the test period, the dynamics of the soil water contents simulated (in the lab or PTF hydrological constants) or those field-measured in PG and CT are similar. The maximum values occur in the spring, when soil moisture is close to FC conditions, and in autumn because of the recharge of the soil water reserve. Minimum values occur in the summer period to varying extents and intensities depending on the input data entered (lab, PTF, and field), the year and the management system.

From Table 7, we can notice that compared to the average value of soil field moisture in the three years, those estimated using the hydrological constants determined in the lab show the lowest percentage difference values in all the months, either for PG or CT; the best simulation is, anyway, observed in the PG treatment. On the contrary, those returned when employing PTF show a higher percentage of difference values, which were all negative in both treatments, indicating an overall underestimation of soil moisture contents. In addition, it is interesting to note that Figure 1a,b show how the annual water stress risk, obtained using hydrological constants measured in the laboratory or estimated via PTF, matches, in most cases, the field measurements, differing by one class at most.

Table 7. Monthly percentage differences between the mean values of simulated and field-measured soil water content on the test period for both treatments (PG and CT) and types of hydrological data (LAB and PTF) used.

Treatment	Hydrological Data	A	M	J1	J2	J	A	S	O	N
PG	PTF	−7.1	−13.6	−11.1	−13.0	−24.1	−21.0	−6.4	−9.4	−1.2
	LAB	1.3	−4.5	−0.9	0.6	−6.9	1.4	5.9	3.1	4.4
CT	PTF	−17.3	−18.9	−19.9	−24.8	−32.4	−32.6	−11.5	−17.2	−11.2
	LAB	3.1	2.1	2.4	0.7	−2.7	−1.0	7.3	6.9	8.1

For CT, the model underestimates the annual stress risk only in 2021, indicating "high" instead of "very high". In PG, the performance is more articulated and dependent on the type of hydrological constants used. When using those obtained by laboratory analysis, the model results coincide with the field observations, apart from the year 2020, for which the model indicates "moderate" instead of "negligible" stress. When hydrological constants are estimated by PTFs, the risk of stress in both 2021 and 2022 is underestimated: "high" instead of "very high" and "moderate" instead of "high", respectively. The climate of 2021, characterized by a prolonged summer drought, highlights how soil may face difficulties in replenishing the water reserve in autumn (October in particular, see Figure 1a,b. These large volumes of rainwater cannot be readily stored in the soil also because the water flows do not occur through the entire soil volume, probably due to the presence of preferential flow pathways generated in fine-textured soils by the shrinking process during summer. In these circumstances, surface runoff prevails over infiltration. The model is not able to simulate this inertia of the soil system because it considers the emptying and replenishing velocity of the water reserve to be uniform. This is the reason why, in October 2021, the stress highlighted by field measurements was more severe than the simulated one; this behavior has been observed for both management systems and lab-measured or PTF-estimated hydrological constants.

3.1.3. Vine Production

The results relating to the production components and the Ravaz index [49] for each year are reported in Table 8.

Table 8. Vine yield components under different soil management: (PG—permanent grass cover, and CT—continuous tillage) during the study period (2020–2022).

Year	Yield (kg/Vine)		Berry Weight (g)		Cluster/Vine (n)		Ravaz Index	
	Mean	St.Dev.	Mean	St.Dev.	Mean	St.Dev.	Mean	St.Dev.
PG								
2020	2.23	±0.88	2.21	±0.21	8.00	±2.23	5.19	±0.95
2021	1.35	±0.64	1.58	±0.04	8.56	±1.67	3.31	±1.5
2022	0.66	±0.29	1.62	±0.25	7.40	±2.06	1.88	±0.2
CT								
2020	1.31	±0.57	2.06	±0.17	4.89	±1.45	4.83	±4.42
2021	1.26	±0.67	1.81	±0.13	6.55	±2.11	4.68	±3.16
2022	0.73	±0.57	1.75	±0.23	6.80	±1.70	2.54	±1.19

None of the production variables considered showed statistical differences between the different managements during the trial period. Considering that production and water availability are correlated [55], based on the outputs provided by the model for the different treatments, we expected that the yield components were also not influenced by the management system. The vine production components, mainly in PG, were very different in the three years. In 2020, when the risk of stress is negligible; PG tends to show better results than CT. Nevertheless, in 2021, when the risk of water stress increased (very high class), in PG, the vine yield drastically decreased, and the Ravaz index assumed a critical value (<4) [49].

In 2022, a year in which moderate water stress was associated with high heat stress, the treatments showed a decrease in both vine yield and Ravaz index. These results highlight how climatic conditions, the cause of abiotic and biotic stress, have a major impact on production; the choice of the type of soil management and the methods of application can help reduce this impact, but it is necessary to foresee already from the planting phase the possibility of adopting other management strategies that facilitate the adaptation to the ongoing climate change.

3.2. Model Application at Farm Scale

3.2.1. Results of Geographical and Pedological Data Processing

Table 9 illustrates the geographical characteristics of the TSU, along with their soil textural class and WRB classification.

According to RCP8.5, the mean annual precipitation remained unchanged (about 835 mm), with respect to the reference thirty-year period (1991–2020), while the mean annual temperature is expected to increase from 13.9 to 15.9 °C. The warming effect was reflected in the trend of the Thornthwaite thermal index (Im), with the humid climate class, initially dominant in the study area (91% of the surface), which is reduced to 34% in the thirty-year period 2021–2050; on the contrary, the subhumid class increases, reaching 66% of the farm surface.

Table 10 lists the values of the main physical and hydrological properties related to the 0–0.75 m soil depth in the different TSUs; the coefficients A and B of Equations (A17) and (A18) (see Appendix A) are also reported.

Table 9. Mean values of altitude and slope (standard deviation in brackets), prevailing aspect (N = North; E = East; S = South; W = West) and row orientation (U = up-and-down; O = oblique) in the different typological soil units (TSU); TSU area, textural class (CL = Clay Loam; C = Clay; SiCL = Silty Clay Loam; SCL = Sandy Clay Loam; SL = Sandy Loam; SiC = Silty Clay) and WRB soil classification [46] are also reported.

TSU	Altitude (m asl)	Slope (%)	Aspect	Row Orientation	Area (ha)	Textural Class (USDA)	Soil Classification (WRB)
AGR1	429.3 (14.4)	9.2 (1.7)	NW, S	U	70.3	CL	Skeleti Haplic Calcisols
AGR2	417.2 (12)	6.7 (1.3)	S, W	O	13.9	C	Hypocalcic Calcisols (Clayic)
ARG	319.1 (0.4)	8 (3)	SW	U	2.7	CL	Alcali Haplic Cambisols (Siltic)
CAS	274.0 (2.7)	10.8 (0.5)	W	U	13.1	SiCL	Skeleti Haplic Cambisols (Eutric)
CAST	461.8 (24.5)	10.5 (2.7)	SW, W, E	U	37.7	SCL	Skeleti Haplic Regosols
CEN1	306.8 (2.8)	13.5 (1.2)	W, SW	U	4.7	SCL	Thapto Luvi Haplic Cambisols (Ruptic)
CEN2	303.6 (10.9)	12.7 (1.6)	SW	O	2.4	C	Profondi Cutanic Luvisols (Hypereutri c)
GRO	439.7 (15.9)	11 (1.4)	SW, NE	U	16.5	CL	Skeleti Haplic Cambisols
LEC1	324.1 (6.8)	7.9 (0.6)	SE	U	2.5	CL	Rupti Cutanic Luvisols (Hypereutric)
LEC2	320.5 (5.2)	8.7 (1)	SE	U	5.1	SL	Eutri Brunic Arenosols
MIN	319.2 (14.8)	12.1 (5.8)	NW, W	U	3.8	C	Eutri Endogleyic Stagnosols (Clayic)
NEB	338.5 (0)	7.3 (0)	NW	U	0.8	SCL	Eutri Haplic Cambisols (Chromic)
PIA1	242.9 (6.1)	4.6 (0.7)	SW	U	11.6	CL	Manganiferri Luvic Stagnosols (Clayic)
PIA2	252.3 (4.7)	6.2 (2.9)	W	U	1.3	C	Cutani Vertic Luvisols (Hypereutric)
SLC	368.8 (37.1)	5.8 (0.2)	SE	O	1.8	C	Cutani Vertic Luvisols (Hypereutric)
TAR1	464.6 (14.9)	6.6 (1.4)	S	U	11.7	SL	Colluvi Haplic Arenosols (Hypoluvic)
TAR2	465.9 (14.9)	11.3 (3.4)	SE	O	4.6	L	Eutri Haplic Cambisols (Skeletic)
TAR3	440.2 (27.1)	7.6 (3.7)	E	U	2.7	SL	Eutri Haplic Arenosols (Transportic)
TOR	347.5 (16.1)	7.9 (2.8)	S, SW, W	O	38.7	SiC	Calcari Haplic Cambisols (Skeletic)

Table 10. Main physical and hydrological properties of each typological soil unit (TSU). (HSG: hydrological soil group [38]; H: soil depth; SK: Skeleton content on a volume basis; A and B: coefficients moisture tension [44]; FC: field capacity; WP: wilting point; AWC: Available Water Content).

TSU	HSG	H (m)	SK (%v)	Sand (%w)	Clay (%w)	A	B	FC (mm)	WP (mm)	AWC (mm)
AGR1	D	0.75	29.7	28.1	38.0	1.43×10^{-4}	−7.49	187.3	112.7	74.6
AGR2	D	0.75	10.0	19.3	49.5	1.34×10^{-4}	−9.23	289.3	191.5	97.8
ARG	D	0.75	2.0	29.2	31.9	2.57×10^{-4}	−6.35	237.9	130.7	107.2
CAS	D	0.75	19.0	14.0	37.6	5.44×10^{-4}	−6.57	228.9	128.2	100.7
CAST	B	0.75	39.7	48.0	33.1	1.53×10^{-5}	−8.14	132.6	83.1	49.5
CEN1	C	0.75	10.0	50.7	21.7	7.12×10^{-5}	−6.14	170.6	91.8	78.8
CEN2	D	0.75	5.5	26.0	47.8	6.91×10^{-5}	−9.37	286.8	191.0	95.8
GRO	C	0.75	52.5	30.3	39.1	1.03×10^{-4}	−7.78	126.2	77.4	48.8
LEC1	C	0.75	0.7	37.6	34.2	6.74×10^{-5}	−7.45	237.9	142.7	95.2
LEC2	C	0.75	6.0	70.9	11.1	4.38×10^{-5}	−5.36	133.0	65.3	67.7
MIN	D	0.75	5.0	24.8	49.8	6.93×10^{-5}	−9.73	298.2	201.7	96.5
NEB	C	0.75	25.0	48.0	30.1	2.39×10^{-5}	−7.56	159.3	96.3	63.0
PIA1	D	0.75	10.0	31.1	36.9	1.19×10^{-4}	−7.41	231.3	138.4	92.9
PIA2	D	0.75	18.0	34.9	42.5	3.47×10^{-5}	−8.97	221.2	144.6	76.6
SLC	D	0.75	18.0	34.9	42.5	3.47×10^{-5}	−8.97	221.2	144.6	76.6
TAR1	C	0.75	10.0	63.2	14.8	4.83×10^{-5}	−5.69	142.6	73.0	69.6
TAR2	C	0.75	25.0	46.0	21.2	1.41×10^{-4}	−5.70	144.0	73.9	70.1
TAR3	C	0.75	10.0	63.8	17.6	2.27×10^{-5}	−6.32	148.1	81.1	67.0
TOR	D	0.75	25.0	18.3	40.7	3.13×10^{-4}	−7.30	216.7	128.6	88.1

3.2.2. Model Results in View of Planning New Vineyards Under Future Climate Scenario

Starting from soil and geographical information, the water balance for young vine plants is elaborated and described in Table 11, where each soil unit data refers to the application of the model to the vineyard with the largest extension.

In Table 11, all cases with an overall negligible annual risk have only one moderate risk, which always occurs in August, the month that induces the most severe water stress. Vineyards with annual moderate risk generally have H risk in August and July. Finally, all vineyards with high annual risk show a monthly H and VH risk in July and August, respectively. The attribution of a different annual water stress risk class to the TSUs is due to the combination of soil hydrological properties (AWC) with potential evapotranspiration (PEc). Since the climate is quite homogeneous within the farm, PEc mainly differs according to the geomorphological characteristics (vineyard aspect, altitude, and slope). Additionally, aspects seem to play a major role. In fact, vineyards with NW, NE, or W aspects generally have a negligible annual risk class often associated with the lowest PEc values in July and August. Moreover, in these vineyards, the highest evapotranspiration demand corresponds

to the highest AWC values and vice versa. Vineyards showing the highest PEc values are exposed to SE or SW and are associated with AWC values among the lowest, falling into the "High" water stress risk class.

Table 11. Modeled monthly and annual water stress risk for young vineyards to be planted in the different TSUs under a future climate scenario (2021–2050). Vineyard aspect (N = North; E = East; S = South; W = West), total potential evapotranspiration (PEc) from June to August, and AWC (0–0.35 m) are also displayed.

TSU	Apr	May	Jun 1	Jun 2	Jul	Aug	Sept	Oct	Nov	Annual Water Stress Risk	Vineyard Aspect	PEc (Jun–Aug) (mm)	AWC (mm)
	Bud Break	Growth of Vine Shoot				Maturation			Falling of Leaves and Root Growth				
	<0.2 None	<0.2 None				0.2–0.4 Moderate			<0.2 None				
CAS	N	N	N	N	N	M	N	N	N	Negligible	W	442	50
GRO	N	N	N	N	N	M	N	N	N	Negligible	NE	364	27
AGR2	N	N	N	N	N	M	N	N	N	Negligible	W	399	45
MIN	N	N	N	N	N	M	N	N	N	Negligible	W	427	44
NEB	N	N	N	N	N	M	N	N	N	Negligible	NW	373	30
AGR1	N	N	N	N	H	H	N	N	N	Moderate	S	484	34
TOR	N	N	N	N	N	H	N	N	N	Moderate	SW	443	41
CAST	N	N	N	N	H	H	N	N	N	Moderate	E	467	29
PIA1	N	N	N	N	H	H	N	N	N	Moderate	SW	490	44
LEC2	N	N	N	N	H	H	N	N	N	Moderate	SE	479	30
TAR1	N	N	N	N	H	H	N	N	N	Moderate	S	486	32
SLC	N	N	N	N	H	H	N	N	N	Moderate	SE	493	39
TAR3	N	N	N	N	N	H	N	N	N	Moderate	E	425	29
LEC1	N	N	N	N	H	H	N	N	N	Moderate	SE	503	42
CEN2	N	N	N	N	H	H	N	N	N	Moderate	SW	480	45
PIA2	N	N	N	N	H	H	N	N	N	Moderate	W	478	39
ARG	N	N	N	N	H	H	N	N	N	Moderate	SW	505	49
CEN1	N	N	N	N	H	VH	N	N	N	High	SW	534	38
TAR2	N	N	N	N	H	VH	N	N	N	High	SE	534	33

With regard to the simulation for the future scenario (2021–2050), Figure 2a illustrates the distribution of farm areas (ha) under different stress risk classes. Almost 55% of the farm area falls into the moderate risk class, 32% into the negligible one and around 13% into the high one.

In Figure 2b, for each TSU (Table 9), the distribution of vineyard areas under different annual water stress risk are displayed, along with the PEc values (mm), from June to August. Only the largest TSUs are shown. In the figure, they are listed for each TSU.

The model provides different results for the same TSU (identical soil characteristics) because of different geomorphological conditions which modify the potential evapotranspiration values. CAS and PIA1 TSUs are exceptions because, being that the geographical attributes of their vineyards are characterized by a low variability, they are entirely described by a unique water stress risk class: CAS TSU falls in the negligible class because of their highest AWC value and relatively low PEc; PIA1 TSU falls entirely in the moderate class because of their intermediate AWC and PEc values.

TSUs showing areas with three different risk classes (AGR1, CAST, GRO, and TOR) have greater variability in altitude and slope, and/or contrasting aspects (Table 9). The wide variability of geomorphological conditions detected in AGR1, CAST, and GRO determines the occurrence of cases of negligible risk, though these UTSs are characterized by a low AWC [56]. In particular, this occurs whenever the vineyard aspect is NW, W, and NE, respectively.

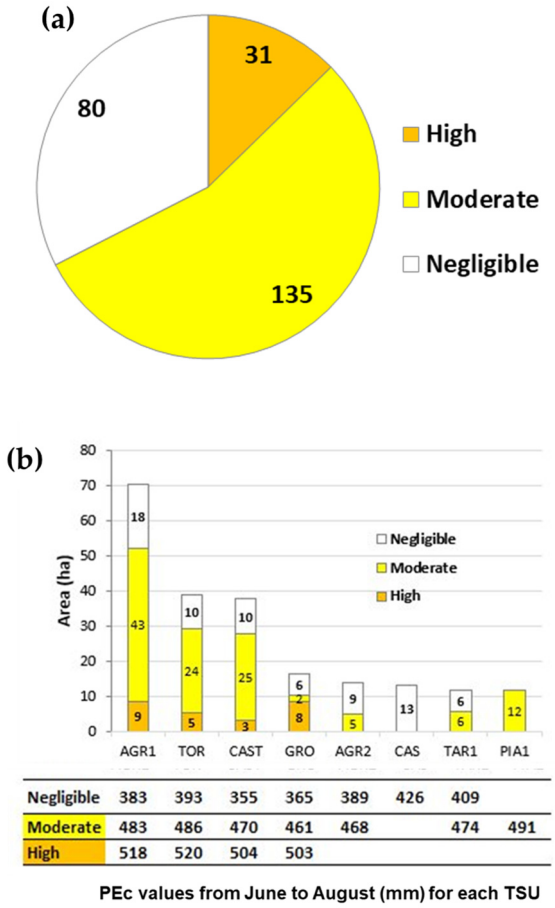

Figure 2. (**a**) Distribution of farm areas (ha) under different stress risk classes; (**b**) vineyard areas (ha) under different annual water stress risk classes in the largest TSUs. PEc values (mm) from June to August under the future climatic scenario (2021–2050) are listed below.

The importance of soil and water resources and the growing attention of global agricultural policies toward these environmental components [57] make it necessary to raise awareness of the short- and long-term effects resulting from inappropriate management choices. Considering the ongoing climate change [22,58] and that different soil types react differently to management methods [59,60], the identification of the most suitable management practices for different crops in specific pedoclimatic environments is crucial [61].

We believe this model can be a useful decision support system in both the planning and management phases of the vineyard. Whenever the model returns a negligible stress risk, there being no limits depending on the soil and climate conditions, the winegrower will be able to make the appropriate decisions based on other farm strategic objectives. On the contrary, conditions of moderate, or even more high or very high stress, could suggest that farmers could make different choices concerning, in the case of a new vineyard, the planting density, the type of rootstock and cultivar, or the need to design an emergency irrigation system; conversely, in the case of mature vineyard, the modification of the management, for example, intervenes on the type of cover crop or on the duration of the soil coverage period. Furthermore, the winegrower is guided by the model in making decisions regarding the production, e.g., number of buds and canopy management, all this with the aim of maintaining adequate and constant production levels without compromising plants' health.

4. Conclusions

In this study, we illustrate the potential of a monthly scale soil water balance model to be implemented in a DSS, which aims to assist agronomists and winemakers in the

planning and management of vineyards. To this aim, the risk of water stress is used as response variable.

Since it provided reliable outputs, the model would be a useful tool for viticulture, especially considering the ongoing climate change which imposes winegrowers to urgently implement adaptation practices and effective managements.

The main strengths of this tool are:

1. It contributes to fill the gap between wine growers or agronomist consultants and the research sector.
2. It provides ready-to-use decision support models for designing new vineyards.

For these reasons, the model will be available as a module within a Decision Support System (DSS) equipped with a user-friendly interface; no specific skills are required from users, farmers, and technicians, nor the availability to access daily information regarding microclimatic data. To ensure consistency and compatibility in data collection, analysis, visualization, and management, the system will be developed entirely in Python. The Graphical User Interface (GUI), built with the Kivy and KivyMD frameworks, will be available in a desktop version.

A weakness of this soil water balance could be that PE is computed using the Thornthwaite equation and corrected according to Armiraglio et al. [33] and Pierce et al. [41]. Nevertheless, Eto value [43], if available, could be directly entered in the model by the user.

The first version of the model is employed in a Geographic Decision Support System at regional scale [62], directly connected to a soil and climatic database.

Additionally, to increase the robustness of the model further research is needed to validate it on vineyards under different pedoclimatic conditions, plants age and spacing, and inter-row soil management systems.

Author Contributions: Conceptualization, M.C.A., S.P., and N.V.; methodology, M.C.A., S.P., and N.V.; software, M.C.A. and A.O.; validation, M.C.A., S.P., C.B., N.V., R.P., and P.S.; formal analysis, M.C.A., S.P., C.B., N.V., and R.P.; investigation, M.C.A., S.P., C.B., N.V., R.P., and P.S.; data curation, M.C.A., S.P., C.B., A.O., N.V., R.P., and P.S.; writing—original draft preparation, M.C.A. and R.P.; writing—review and editing, M.C.A., S.P., C.B., R.P., and N.V.; funding acquisition, P.S., S.P., and N.V. All authors have read and agreed to the published version of the manuscript.

Funding: This research was funded with the contribution of the Italian Ministry of Agricultural, Food, Forestry and Tourism (MiPAAFT) sub-project "SUVISA-Viticoltura" (AgriDigit program) (DM n. 36510/7305/18 del 20 December 2018).

Data Availability Statement: For privacy reasons, the data presented in this study will be available upon request to the corresponding author.

Acknowledgments: The authors wish to thank the Barone Ricasoli S.p.A. Società Agricola for hosting the trial and Massimiliano Biagi and Jacopo Nannicini for their support in maintaining the experimental sites and for their help in field data collection.

Conflicts of Interest: The authors declare no conflicts of interest. The funders had no role in the design of the study; in the collection, analyses, or interpretation of data; in the writing of the manuscript; or in the decision to publish the results.

Appendix A

Appendix A.1. Potential Evapotranspiration (PE)

The model calculates monthly potential evapotranspiration (*PE*), defined by Thornthwaite [34] in terms of the thermal efficiency index and monthly air temperature. According to this method, *PE* can be calculated for the month *i* through the following equation:

$$PE_i = 0.16 \times \left(\frac{T_i}{I}\right)^{\alpha} \text{ if } T_i > 0;\ PE_i = 0 \text{ if } T_i \leq 0 \quad \text{(A1)}$$

where T is the mean monthly air temperature, and I the thermal Index computed by the Equation (A2)

$$I = \sum_{i=1}^{12} \left(\frac{t_i}{5}\right)^{1.514} \quad \text{(A2)}$$

and the exponent α is determined through the following function of I.

$$\alpha = 6.75 \times 10^{-7} \times I^3 - 7.71 \times 10^{-5} \times I^2 - 1.7921 \times 10^{-2} \times I + 0.49239 \quad \text{(A3)}$$

In the standard procedure, the Thornthwaite balance [34] simply provides an overall result expressed by the Moisture Index (I_m), computed by the following equation:

$$I_m = \left(\frac{P - PE}{PE}\right) \times 100 \quad \text{(A4)}$$

where P and PE are, respectively, the annual precipitation and potential evapotranspiration. I_m index identifies several climatic classes, each characterized by different qualities and agronomic implications.

In our case, no classification is processed, rather greater accuracy at the monthly/phenological scale is sought. In fact, further adjustments have been carried out to improve month by month the assessment of each term of the balance.

Appendix A.2. Exposed Leaf Area (ELA)

In this section a set of formulas to calculate the Exposed leaf Area (*ELA*, $m^2\ ha^{-1}$) by geometric approach for the main trellis systems, is listed:

Vertical trellis (Cordon, Guyot):

$$ELA = \frac{c}{100} \times (2 \times H_l + D) \times \left(\frac{10,000}{E}\right) \quad \text{(A5)}$$

Vertical trellis (Lyra):

$$ELA = \frac{c}{100} \times (2 \times H_l) \times \left(\frac{10,000}{E}\right) \quad \text{(A6)}$$

Tent:

$$ELA = \frac{c}{100} \quad \text{(A7)}$$

Trunk:

$$ELA = \frac{c}{100} \times (\pi \times D \times H_l) \times (n) \quad \text{(A8)}$$

where n is the planting density that is the number of vines per hectare, whereas all the other variables (c, H_l, D, and E are already described at Section 2.1.2.

Appendix A.3. Vine Crop (Kc) and Cover Crop (Kcc) Coefficient Monthly Correction in Relation to Soil Water Avalability

According to the VSIM user Guide [41], a further coefficient, named Cor_j, is monthly applied to reduce *Kcj* values in relation to the soil moisture potential (ψ_{j-1}), calculated on the previous month.

$$Cor_j = \left(1 - \frac{\psi_{j-1} - 0.7}{1.4 - 0.7}\right) \tag{A9}$$

where 0.7 represents the soil water potential (SWP) value (MPa) at which kc_j begins to decrease as a function of soil water content inducing water stress, and 1.4 is the water potential threshold at which kc_j is set equal to zero because of severe stress.

Hence, the monthly kc_j value is corrected (kc_{corj}) as follows:

$$kc_{corj} = Cor_j \times .kc_j \tag{A10}$$

According to the VSIM user Guide [41], also the cover crop coefficient *Kccj* is reduced in relation to the soil moisture of the previous month

$$Kccj \times \left(\frac{SM_{j-1} - 0.6 \times FC}{\mathrm{FC} - 0.6 \times FC}\right) \tag{A11}$$

where SM_{j-1} represents the soil water content value (mm) of the antecedent month, while *FC* is the soil Field Capacity (mm) referred to the rooting depth.

Appendix A.4. Soil Water Dynamics

In every *j*-th month where $(P_{net} - Etc)_j < 0$, soil water storage (ST_j) undergoes a change in relation to both the AWC value, that represents the starting moisture status of soil in January, and the cumulated water loss values (WL_j), month by month, according to the resulting exponential equation:

$$ST_j = AWC \times e^{n \times |WL_j|} \tag{A12}$$

where WL_j is obtained by adding the $(P_{net} - Etc)_j$ amount to the WL_{j-1} value of the antecedent *j*-th month, whereas *n* is calculated through a polynomial equation, depending exclusively on *AWC* [33]. When $(P_{net} - Etc)_j \geq 0$, the following conditions are applied:

$$ST_j = AWC \times WL_j = 0;\ (P_{net} - Etc)_j + ST_{j-1} \geq AWC \tag{A13}$$

$$ST_j = ST_{j-1} + (P_{net} - Etc)_{ij}\ \ WL_j = 0;\ (P_{net} - Etc)_j + ST_{j-1} < AWC \tag{A14}$$

To convert *SM* (mm) into potential ψ (MPa) values, once more the equation of Saxton et al. [44] is employed:

$$\psi = \boldsymbol{A} \times \left\{\frac{SM}{Rd \times \left(1 - \frac{SK}{100}\right)}\right\}^{\boldsymbol{B}} \times \frac{1}{10} \tag{A15}$$

where *SK* is the skeleton content (%vol), is the weighted average of the individual SK_i values as a function of the thickness of each *i*-th horizon; ***A*** and ***B*** are obtained solving the following system of equations:

$$\begin{cases} 0.0333 = \boldsymbol{A} \times \left[\frac{FC}{Rd \cdot \left(1 - \frac{SK}{100}\right)}\right]^{\boldsymbol{B}} \times \frac{1}{10} \\ 1.5 = \boldsymbol{A} \times \left[\frac{WP}{Rd \cdot \left(1 - \frac{SK}{100}\right)}\right]^{\boldsymbol{B}} \times \frac{1}{10} \end{cases} \quad \text{(A16)}$$

where *FC* and *WP* values (mm) referred to the rooting depth. When the hydrological constants are measured, *FC* value must be referred to 0.01 MPa, instead of 0.033 MPa. The solution of that equations system provides the two coefficients:

$$\boldsymbol{A} = \frac{(1.5 \times 10)}{\left[\left(1 - \frac{SK}{100}\right) \times Rd\right]^{\boldsymbol{B}}} \quad \text{(A17)}$$

$$\boldsymbol{B} = \frac{\log\left(\frac{0.0333}{1.5}\right)}{\log\left(\frac{FC_{mm}}{WP_{mm}}\right)} \quad \text{(A18)}$$

References

1. Darouich, H.; Ramos, T.B.; Pereira, L.S.; Rabino, D.; Bagagiolo, G.; Capello, G.; Simionesei, L.; Cavallo, E.; Biddoccu, M. Water Use and Soil Water Balance of Mediterranean Vineyards under Rainfed and Drip Irrigation Management: Evapotranspiration Partition and Soil Management Modelling for Resource Conservation. *Water* **2022**, *14*, 554. [CrossRef]
2. Palliotti, A.; Panara, F.; Silvestroni, O.; Lanari, V.; Sabbatini, P.; Howell, G.; Gatti, M.; Poni, S. Influence of mechanical postveraison leaf removal apical to the cluster zone on delay of fruit ripening in Sangiovese (*Vitis vinifera* L.) grapevines. *Aust. J. Grape Wine Res.* **2013**, *19*, 369–377. [CrossRef]
3. Buesa, I.; Caccavello, G.; Basile, B.; Merli, M.C.; Poni, S.; Chirivella, C.; Intrigliolo, D.S. Delaying berry ripening of Bobal and Tempranillo grapevines by late leaf removal in a semi-arid and temperate-warm climate under different water regimes. *Aust. J. Grape Wine Res.* **2019**, *25*, 70–82. [CrossRef]
4. Garcia, L.; Celette, F.; Gary, C.; Ripoche, A.; Valdés-Gómez, H.; Metay, A. Management of service crops for the provision of ecosystem services in vineyards: A review. *Agric. Ecosyst.* **2018**, *251*, 158–170. [CrossRef]
5. *(EU) 2018/1981*; Commission Implementing Regulation (EU) 2018/1981 of 13 December 2018 Renewing the Approval of the Active Substances Copper Compounds, as Candidates for Substitution, in Accordance with Regulation (EC) No 1107/2009 of the European Parliament and of the Council Concerning the Placing of Plant Protection Products on the Market, and Amending the Annex to Commission Implementing Regulation (EU) No 540/2011 (Text with EEA Relevance). European Commission: Brussels, Belgium, 2018.
6. *(EU) 2021/2115*; Regulation (EU) 2021/2115 of the European Parliament and of the Council of 2 December 2021 Establishing Rules on Support for Strategic Plans to Be Drawn Up by Member States Under the Common Agricultural Policy (CAP Strategic Plans) and Financed by the European Agricultural Guarantee Fund (EAGF) and by the European Agricultural Fund for Rural Development (EAFRD) and Repealing Regulations (EU) No 1305/2013 and (EU) No 1307/2013. European Parliament and of the Council: Brussels, Belgium, 2021.
7. Shackelford, G.E.; Kelsey, R.; Dicks, L.V. Effects of cover crops on multiple ecosystem services: Ten meta-analyses of data from arable farmland in California and the Mediterranean. *Land Use Policy* **2019**, *88*, 104204. [CrossRef]
8. Yousefi, M.; Marja, R.; Barmettler, E.; Six, J.; Dray, A.; Ghazoul, J. The effectiveness of intercropping and agri-environmental schemes on ecosystem service of biological pest control: A meta-analysis. *Agron. Sustain. Dev.* **2024**, *44*, 15. [CrossRef]
9. Knowling, M.J.; Bennett, B.; Ostendorf, B.; Westra, S.; Pellegrino, A.; Edwards, E.J.; Collins, V.; Pagay, D. Grigg. Bridging the gap between data and decisions: A review of process-based models for viticulture. *Agric. Syst* **2021**, *193*, 103209. [CrossRef]
10. Brisson, N.; Gary, C.; Justes, E.; Roche, R.; Mary, B.; Ripoche, D.; Zimmer, D.; Sierra, J.; Bertuzzi, P.; Burger, P.; et al. An overview of the crop model stics. *Eur. J. Agron.* **2003**, *18*, 309–332. [CrossRef]
11. Walker, R.R. VineLOGIC Virtual Vineyard. In *User's Manual Version 2*; CRC for Viticulture Technologies Pty Ltd.: Adelaide, SA, Australia, 2006; ISBN 0-9581057-3-1.
12. Pelak, N.; Revelli, R.; Porporato, A. A dynamical systems framework for crop models: Toward optimal fertilization and irrigation strategies under climatic variability. *Ecol. Model.* **2017**, *365*, 80–92. [CrossRef]
13. Terraclim. Available online: https://www.terraclim.co.za/ (accessed on 21 December 2024).
14. Prevostini, M.; Taddeo, A.V.; Jermini, M.; Linder, C.; Petit, A. Monitoring Scaphoideus titanus and related in-field activities: The experience in Switzerland and France using PreDiVine DSS. In Proceedings of the IOBC-WPRS Conference of the Working Group on Integrated Protection and Production in Viticulture, Vienna, Austria, 20–23 October 2015; pp. 20–23.

15. Rossi, V.; Salinari, F.; Poni, S.; Caffi, T.; Bettati, T. Addressing the implementation problem in agricultural decision support systems: The example of vite.net®. *Comput. Electron. Agric.* **2014**, *100*, 88–99. [CrossRef]
16. Serrano, A.S.; Martínez-Gascueña, J.; Alonso, G.L.; Cebrián-Tarancón, C.; Carmona, M.D.; Mena, A.; Chacón-Vozmediano, J.L. Agronomic Response of 13 Spanish Red Grapevine (*Vitis vinifera* L.) Cultivars under Drought Conditions in a Semi-Arid Mediterranean Climate. *Agronomy* **2022**, *12*, 2399. [CrossRef]
17. Williams, L.E.; Ayars, J.E. Grapevine water use and the crop coefficient are linear functions of the shaded area measured beneath the canopy. *Agric. Forest Meteorol.* **2005**, *132*, 201–211. [CrossRef]
18. Mirás-Avalos, J.M.; Araujo, E.S. Optimization of Vineyard Water Management: Challenges, Strategies, and Perspectives. *Water* **2021**, *13*, 746. [CrossRef]
19. Zufferey, V.; Maigre, D. Vine plant age. I. Influence on physiological behaviour. *Rev. Suis. Vitic. Arbor. Hort.* **2007**, *39*, 257–261.
20. Nader, K.B.; Stoll, M.; Rauhut, D.; Patz, C.; Jung, R.; Loehnertz, O.; Schultz, H.R.; Hilbert, G.; Renaud, C.; Roby, J.P.; et al. Impact of grapevine age on water status and productivity of Vitis vinifera L. cv. Riesling. *Eur. J. Agron.* **2019**, *104*, 10–12. [CrossRef]
21. Deloire, A.; Carbonneau, A.; Wang, Z.; Ojeda, H. Vine and water: A short review. *J. Int. Sci. Vigne Vin* **2004**, *38*, 1–13. [CrossRef]
22. Santos, J.A.; Fraga, H.; Malheiro, A.C.; Moutinho-Pereira, J.; Dinis, L.T.; Correia, C.; Moriondo, M.; Leolini, L.; Dibari, C.; Costafreda-Aumedes, S.; et al. A review of the potential climate change impacts and adaptation options for European viticulture. *Appl. Sci.* **2020**, *10*, 3092. [CrossRef]
23. Carbonneau, A. Aspects qualitatifs. In *Proc. XXVIIth World Congress of Vine and Wine, Bratislava. Traité d'Irrigation*; Tiercelin, J.R., Ed.; Tec et Doc Lavoisier: Paris, France, 1998; 1011p, pp. 258–276.
24. Ojeda, H. Irrigation qualitative de précision de la vigne. *Le Progrès Agric. Vitic.* **2007**, *7*, 133–141.
25. Herceg, A.; Kalicz, P.; Kisfaludi, B.; Gribovszki, Z. A monthly-step water balance model to evaluate the hydrological effects of climate change on a regional scale for irrigation design. *Slovak J. Civ. Eng.* **2016**, *24*, 27–35. [CrossRef]
26. Hong, X.; Guo, S.; Chen, G.; Guo, N.; Jiang, C. A Modified Two-Parameter Monthly Water Balance Model for Runoff Simulation to Assess Hydrological Drought. *Water* **2022**, *14*, 3715. [CrossRef]
27. Mammoliti, E.; Fronzi, D.; Mancini, A.; Valigi, D.; Tazioli, A. WaterbalANce, a WebApp for Thornthwaite–Mather Water Balance Computation: Comparison of Applications in Two European Watersheds. *Hydrology* **2021**, *8*, 34. [CrossRef]
28. Thornthwaite, C.W.; Mather, J.R. Instructions and tables for computing potential evapotranspiration and the water balance: Centerton, N.J., Laboratory of Climatology. *Publ. Climatol.* **1957**, *10*, 185–311.
29. Steenhuis, T.S.; Van der Molen, W.H. The Thornthwaite-Mather procedure as a simple engineering method to predict recharge. *J. Hydrol.* **1986**, *84*, 221–229. [CrossRef]
30. Barros, F.d.C.; Martins, S.d.C.F.; Lyra, G.B.; Silva, L.D.B.d.; Francisco, J.P.; Abreu, M.C.d.; Lyra, G.B. Thornthwaite and Mather soil water balance model adapted for estimation of real evapotranspiration of the pasture. *Eng. Na Agric.* **2021**, *29*, 146–156. [CrossRef]
31. Dourado-Neto, D.; van Lier, J.; Metselaar, K.; Reichardt, K.; Nielsen, D.R. General procedure to initialize the cyclic soil water balance by the Thornthwaite and Mather method. *Sci. Agric.* **2010**, *67*, 87–95. [CrossRef]
32. Zhu, G.; Qin, D.; Tong, H.; Liu, Y.; Li, J.; Chen, D.; Wang, K.; Hu, P. Variation of Thornthwaite moisture index in Hengduan Mountains, China. *Chin. Geogr. Sci.* **2016**, *26*, 687–702. [CrossRef]
33. Armiraglio, S.; Cerabolini, B.; Gandellini, F.; Gandini, P.; Andreis, C. Calcolo informatizzato del bilancio idrico del suolo. *Nat. Brescia. Ann. Mus. Civ. Sc. Nat. Brescia* **2003**, *33*, 209–216.
34. Thornthwaite, C.W.; Mather, J.R. The water balance. *Climatology* **1955**, *8*, 1–104.
35. Wu, W.Y.; Yang, Z.L.; Barlage, M. The Impact of Noah-MP Physical Parameterizations on Modeling Water Availability during Droughts in the Texas–Gulf Region. *J. Hydrometeorol.* **2021**, *22*, 1221–1233. [CrossRef]
36. McCabe, G.J.; Markstrom, S.L. *A Monthly Water-Balance Model Driven by a Graphical User Interface*; U.S. Geological Survey Open-File Report 2007-1088; US Geological Survey: Reston, VA, USA, 2007; 6p. [CrossRef]
37. Ferguson, B.K. Estimation of Direct Runoff in the Thornthwaite Water Balance. *Prof. Geogr.* **1996**, *48*, 263–271. [CrossRef]
38. USDA-SCS (U.S. Department of Agriculture-Soil Conservation Service). *SCS National Engineering Handbook, Section 4, Hydrology. Chapter 10, Estimation of Direct Runoff from Storm*; USDA-SCS: Mountain View, WY, USA, 1972.
39. Roux, S.; Delpuech, X.; Daudin, G.; Brun, F.; Wery, J.; Wallach, D. Providing user-oriented uncertainty information with a vineyard model used for irrigation decisions. In *Practical Applications of Agricultural System Models to Optimize the Use of Limited Water*; Ahuja, L.R., Ma, L., Lascano, R.J., Eds.; Advances in Agricultural Systems Modeling; ASA, SSSA, CSSA: Madison, WI, USA, 2014; pp. 183–208. [CrossRef]
40. Abou Ali, A.; Bouchaou, L.; Er-Raki, S.; Hssaissoune, M.; Brouziyne, Y.; Ezzahar, J.; Khabba, S.; Chakir, A.; Labbaci, A.; Abdelghani, C. Assessment of crop evapotranspiration and deep percolation in a commercial irrigated citrus orchard under semi-arid climate: Combined Eddy-Covariance measurement and soil water balance-based approach. *Agric. Water Manag.* **2023**, *275*, 107997. [CrossRef]
41. Pierce, L.; Nemani, R.; Johnson, L. VSIM—Vineyard Soil Irrigation Model—User's Guide. 2006. Available online: https://www.scribd.com/document/70248217/Vsim-030106-Guide (accessed on 21 December 2024).

42. Reynolds, A.G.; Vanden Heuvel, J.E. Influence of Grapevine Training Systems on Vine Growth and Fruit Composition: A Review. *Am. J. Enol. Vitic.* **2009**, *60*, 251–268. [CrossRef]
43. Allen, R.G.; Pereira, L.S.; Raes, D.; Smith, M. *Crop Evapotranspiration—Guidelines for Computing Crop Water Requirements*; FAO Irrigation and Drainage Paper 56; FAO: Rome, Italy, 1998; Volume 300, p. D05109.
44. Saxton, K.E.; Rawls, W.J.; Romberger, J.S.; Papendick, R.I. Estimating generalized soil-water characteristics from texture. *Soil Sci. Soc. Am. J.* **1986**, *50*, 1031–1036. [CrossRef]
45. Priori, S.; Costantini, E.A.C. Soil Mapping. In *Beyond Zoning. A Three Year Study at Castello di Brolio*; Costantini, E.A.C., Ed.; Polistampa: Firenze, Italy, 2013; pp. 23–41. ISBN 978-88-596-1224-7.
46. IUSS Working Group WRB. *World Reference Base for Soil Resources*; World Soil Resources Reports 103; FAO: Rome, Italy, 2006.
47. Andrenelli, M.C.; Fiori, V.; Pellegrini, S. Soil particle-size analysis up to 250 micron by X-ray granulometer: Device set-up and regressions for data conversion into pipette-equivalent values. *Geoderma* **2013**, *192*, 380–393. [CrossRef]
48. Sanesi, G. *Guida Alla Descrizione Del Suolo. Progetto Finalizzato "Conservazione del Suolo"*; CNR: Firenze, Italy, 1977; p. 157.
49. Ravaz, L. Sur la brunissure de la vigne. *Les Comptes Rendus L'académie Des Sci.* **1903**, *136*, 1276–1278.
50. Marchi, M.; Bucci, G.; Iovieno, P.; Ray, D. ClimateDT: A Global Scale-Free Dynamic Downscaling Portal for Historic and Future Climate Data. *Environments* **2024**, *11*, 82. [CrossRef]
51. Schwalm, C.R.; Glendon, S.; Duff, P.B. RCP8.5 tracks cumulative CO_2 emissions. *Proc. Natl. Acad. Sci. USA* **2020**, *117*, 19656–19657. [CrossRef] [PubMed] [PubMed Central]
52. *SPSS Statistics Software*; V20; IBM SPSS Statistics: Chicago, IL, USA, 2009.
53. Bagnouls, F.; Gaussen, H. Dry Season and Xerothermic Index. *Bull. Société d'Histoire Nat. Toulouse* **1953**, *88*, 193–239.
54. Lozano-Parra, J.; Pulido, M.; Lozano-Fondón, C.; Schnabel, S. How do Soil Moisture and Vegetation Covers Influence Soil Temperature in Drylands of Mediterranean Regions? *Water* **2018**, *10*, 1747. [CrossRef]
55. Martínez-Vidaurre, J.M.; Pérez-Álvarez, E.P.; García-Escudero, E.; Ramos, M.C.; Peregrina, F. Differences in soil water holding capacity and available soil water along growing cycle can explain differences in vigour, yield, and quality of must and wine in the DOCa Rioja. *Horticulturae* **2024**, *10*, 320. [CrossRef]
56. Costantini, E.A.C. (Ed.) *Manual of Methods for Soil and Land Evaluation*; Science Publisher: Enfield, NH, USA, 2009; p. 549. ISBN 978-1-57808-571-2.
57. FAO. *The State of the World's Land and Water Resources for Food and Agriculture—Systems at Breaking Point. Main Report*; FAO: Rome, Italy, 2022. [CrossRef]
58. IPCC. *Climate Change 2022: Impacts, Adaptation, and Vulnerability. Contribution of Working Group II to the Sixth Assessment Report of the Intergovernmental Panel on Climate Change*; Cambridge University Press: Cambridge, UK; New York, NY, USA, 2022.
59. Singh, R.; Srivastava, P.; Verma, P.; Singh, P.; Bhadouria, R.; Singh, V.K.; Singh, H.; Raghubanshi, A.S. Chapter 21. Exploring soil responses to various organic amendments under dry tropical agroecosystems. In *Climate Change and Soil Interactions*; Prasad, M.N.V., Pietrzykowski, M., Eds.; Elsevier Ltd.: Amsterdam, The Netherlands, 2020; pp. 583–612. [CrossRef]
60. Nazaries, L.; Singh, B.P.; Sarker, J.R.; Fang, Y.Y.; Klein, M.; Singh, B.K. The response of soil multi-functionality to agricultural management practices can be predicted by key soil abiotic and biotic properties. *Agric. Ecosyst. Environ.* **2021**, *307*, 107206. [CrossRef]
61. Grigorieva, E.; Livenets, A.; Stelmakh, E. Adaptation of Agriculture to Climate Change: A Scoping Review. *Climate* **2023**, *11*, 202. [CrossRef]
62. Barbetti, R.; Criscuoli, I.; Valboa, G.; Vignozzi, N.; Pellegrini, S.; Andrenelli, M.C.; L'Abate, G.; Fantappiè, M.; Orlandini, A.; Lachi, A.; et al. A Regional 100 m Soil Grid-Based Geographic Decision Support System to Support the Planning of New Sustainable Vineyards. *Agronomy* **2024**, *14*, 596. [CrossRef]